Revision 2

Evidence for multiple diamondite-forming events in the mantle

Sami Mikhail[1], Daniel Howell[2], Francis M McCubbin[3]

[1]Geophysical Laboratory, Carnegie Institution of Washington, 5251 Broad Branch Rd., N.W, Washington, DC 20015, USA (smikhail@ciw.edu)

[2]ARC Center of Excellence for Core to Crust Fluid Systems (CCFS) and GEMOC, Department of Earth & Planetary Science, Macquarie University, NSW 2109, Australia

[3]Institute of Meteoritics, Department of Earth and Planetary Sciences, University of New Mexico, Albuquerque, New Mexico 87131-1126, U.S.A.

Abstract

A collection of 35 diamondite samples (polycrystalline diamond aggregates, sometimes referred to as framesites), assumed to be from southern Africa, have been studied to investigate their infrared (IR) spectroscopic characteristics. Due to the abundance of sub-micron, interlocking diamonds (polycrystalline) with mineral and fluid inclusions within the diamond material affecting their transparency, only fragments from 10 of the samples provided high quality data. The IR spectra showed a wide range of generally high nitrogen concentrations (386 – 2677 ppm), with a full range of nitrogen aggregation states, from pure IaA to pure IaB. Platelet characteristics were interpreted as being regular (i.e. not having been affected by

deformation and/or heating events), meaning the nitrogen aggregation data could be interpreted with confidence. Surprisingly, the platelet data showed a positive correlation between their intensity (integrated area) and peak position. The primary hydrogen band (at 3107 cm^{-1}) and secondary band (at 1405 cm^{-1}) are both often present in the samples' spectra, but show no correlation with any other characteristic. There is also no correlation between the samples' paragenesis (as defined by their garnet chemistry) and any of the IR characteristics. Whilst we have no independent determination of the samples mantle residence age, nor the temperature they resided at, we infer that diamondite formation has occurred episodically over a large time frame in single and distinct growth events (as opposed to over a short time frame but over a large depth / temperature range). This idea is more in keeping with the theory that C-O-H diamond- (and diamondite-) forming fluids are the result of localized small volume processes. Interestingly, one sample contained fluid inclusions that exhibited a water:carbonate molar ratio (~0.8), similar to the saline and silicic end members of the monocrystalline diamond-forming fluid chemical spectrum.

Keywords: polycrystalline diamond, framesite, infrared spectroscopy, nitrogen aggregation, C-O-H mantle fluids.

1. Introduction

Diamondites are polycrystalline mantle xenoliths that are associated with kimberlites. Their occurrence has been reported from a number of kimberlite pipes in southern Africa (Venetia, Premier, Jwaneng, Orapa; see Dobosi and Kurat 2002)

and Siberia (Mir, Aikhal; Sobolev 1977). They consist predominantly of randomly oriented diamond crystals of varying sizes (Kurat and Dobosi 2000), along with varying amounts of silicates (garnet, clinopyroxene), oxides (magnetite, rutile, ilmenite), sulphides (pyrrhotite), native metals (iron) and Fe-carbides as intergrowths and inclusions (Dobosi and Kurat 2002; Gurney and Boyd 1982; Jacob et al. 2000, 2004, 2011; Kirkley et al. 1991). These minerals can help define a formation paragenesis (source rock affinity). In monocrystalline diamonds, peridotitic and eclogitic parageneses are most prevalent, with a small number classified as websteritic (Stachel & Harris 2008). While polycrystalline diamonds are relatively understudied compared to monocrystalline samples, websteritic and eclogitic and parageneses dominate (see Mikhail et al. 2013 and references therein).

Some workers argue the crystallization histories of diamondites are distinctly different from monocrystalline diamonds (see Heaney et al. 2005 for a review) and several different theories have been proposed to account for their formation at specific localities. Some invoke a subduction component (Burgess et al. 1998; Honda et al. 2004; Mikhail et al. 2013), while others are less convinced by the contribution of crustal material and rely more upon upper mantle melts/fluids that contain a carbonatitic component (Kurat & Dobosi 2000; Jacob et al. 2000; Maruoka et al. 2004; Gautheron et al. 2005). At present, no formation age data has been obtained from diamondites. Some of the aforementioned studies loosely connect their diamondite samples' formation to ancient episodes of monocrystalline diamond growth (e.g. Honda et al. 2004), while other propose a much younger age, with

66 formation occurring only shortly before kimberlite emplacement (e.g. Jacob et al.
67 2000).

68 Nitrogen aggregation data provides a qualitative method to investigate the mantle
69 residence time and temperature of diamonds (Evans and Harris 1989; Mendelssohn
70 and Milledge 1995). Nitrogen is the most common substitutional impurity found in
71 natural diamonds and forms the basis of their classification. Type I diamonds
72 contain nitrogen, while Type II diamonds are nominally nitrogen free (<10 ppm as
73 determined by Fourier Transform infrared (FTIR) spectroscopy). Nitrogen is
74 relatively mobile in the diamond lattice at mantle pressure and temperature
75 conditions. As a result the defects evolve over time from single nitrogen (C centres,
76 Type Ib; Dyer et al. 1965), to pairs of nitrogen atoms (A centres, Type IaA; Davies
77 1976), to 4 nitrogen atoms tetrahedrally arranged about a vacancy (B centres, Type
78 IaB; Evans and Qi 1982), in a process referred to as nitrogen aggregation. The first
79 step in this progress (C to A centre aggregation) occurs quite rapidly (<1 Ma), while
80 the second step (A to B centre) occurs much more slowly (over Ga). This A to B
81 centre aggregation follows a second-order kinetics law (Chrenko et al. 1977), which
82 means it can be used to estimate either the duration the diamond has resided in the
83 mantle for, or the average temperature at which it resided (assuming the other is
84 known). Platelets, planar interstial carbon aggregates found on the {100} crystal
85 planes (Humble, 1982), are the byproduct of B centre formation and show a linear
86 relationship with B centre absorption (Woods, 1986). However, these features are
87 prone to degradation during deformation and/or heating events (Woods, 1986).

In this study we provide the first documentation of the FTIR impurity characteristics of some of the diamond material that make up diamondites. We use this data, and the time and temperature relationship of nitrogen aggregation, to assess the temporal and depth constraints of diamondite formation, as well as investigate any indications of their deformation history.

2. Samples

A collection of 35 diamondites, held at the Department of Mineralogy and Petrography, Naturhistorisches Museum Vienna, Austria, were used in this investigation. Detailed descriptions of samples from this collection are provided by Kurat and Dobosi (2000) and Dobosi and Kurat (2002). Fragments of individual crystals were obtained from these samples by mechanically breaking small pieces off each sample. However, the transparency of the diamond crystals that form the diamondite can be highly variable, depending upon the concentration of included material (minerals and/or fluids; Figure 1). As a result, despite analyzing fragments from all 35 diamondite samples, only 10 of them yielded high quality FTIR spectra. The data presented below comes from 35 fragments of 10 of the diamondite samples (Table 1).

To determine the paragenesis of the diamondite samples, the garnet discrimination diagram of Aulbach et al. (2002) was used. Of the samples analysed, 5 are of websteritic and 2 of peridotitic paragenesis (Dobosi and Kurat 2010); 3 samples had an absence of silicates and are therefore classified as unknown (Table 1). As these samples were purchased from a gem dealer, the exact geographical origin of these

diamondite samples is unknown. However, previous workers (Kurat and Dobosi 2000) inferred them to be from southern Africa, as similar samples have been described from the Orapa, Jwaneng (Botswana) and Venetia (South Africa) kimberlites (Gurney and Boyd 1982; McCandless et al. 1989; Kirkley et al. 1991; Jacob et al. 2000).

3. Analytical technique

Infrared spectroscopic measurements were conducted at room temperature in transmittance mode on a Nicolet Nexus 650 Fourier Transform infrared spectrometer with Continuum microscope configured for the mid- to near-IR (Institute of Meteoritics, University of New Mexico) using the procedures employed by Mason et al. (2009). Both the IR objective and interior of the IR bench unit was in an atmosphere purged of H_2O and CO_2, which eliminated atmospheric absorption features. Data were collected over the mid-IR (400-4000 cm^{-1}) region using a Globar source, KBr beam splitter, and deuterated triglycine sulfate (DTGS) detector. Approximately 256 scans were performed for each IR spectrum acquired at a resolution of 4 cm^{-1}. Background spectra were collected under the same analytical conditions before each analysis and used to calculate absorbance by dividing each sample spectrum and then taking the base-10 logarithm.

The IR spectra were deconvoluted using the excel version of the DiaMap software (Howell et al. 2012a, b). Uncertainties on each component are as such; nitrogen content and aggregation state – ± 10%, platelet intensity [I(B´)] – ± 20%, platelet band position and height – ± 1cm^{-1}, hydrogen-related band heights at 3107 and

1405 cm^{-1} – ± 1cm^{-1}. While all of these uncertainties are very conservative, the reason for the large uncertainty on I(B´) is due to the exceptionally large platelet features that occur in some of the spectra and how variations in the baseline can significantly affect the result. Reproducibility of this dataset is however maintained by the standardizing effect that the DiaMap software has on spectral deconvolution (Howell et al. 2012a, b).

4. Results

The data obtained from the FTIR spectra for all the samples are presented in Table 1. The range of nitrogen concentrations within the sample set is large and consistently above the average nitrogen abundance seen for monocrystalline diamonds (ca. 200-300 ppm; Cartigny, 2005). For example, Dia020 has the lowest nitrogen abundances of 386 ppm, and sample Dia073B has the highest nitrogen abundances of 2677 ppm (Table 1). In general, multiple analyses of the nitrogen content from different fragments of the same sample provide data that are within uncertainty of each other. Overall nitrogen aggregation states (expresses as the % B-centers) vary from 0 to 100% (Table 1). Two of the samples show nitrogen aggregation states between 0 and 8.6% (Dia070 and Dia068), the remaining samples show aggregation states with >40% B-centers present, and samples Dia057 and Dia075 show fully aggregated nitrogen (100% IaB; Figure 2). We observe no relationship between garnet paragenesis and the nitrogen aggregation state of the diamond from these diamondites.

When the primary hydrogen-related band was observed at 3107 cm^{-1}, the secondary band at 1405 cm^{-1} was also observed. Some additional bands were observed at 2924 and 2855 cm^{-1} in samples Dia019 and Dia066, which may also be related to hydrogen (Woods and Collins 1983). The intensity of the primary hydrogen band shows no correlation with any of the other impurity data, but it is important to note that this feature does not provide quantitative data regarding hydrogen concentration due to the possibility of non-IR-active hydrogen also being contained within the diamond (Connell et al. 1998).

Finally, despite sample selection being based on optical transparency, one spectrum (Dia066_2) revealed clear evidence of fluid inclusions (Figure 3). The strong hydrous band (between 2750 – 3700 cm^{-1}) and weaker carbonate band (1420 – 1500 cm^{-1}) can provide semi-quantitative concentration data (see method of Navon et al. 1988; their Table 1, which was followed here). In Dia066_2 there is approximately 104 ppm H_2O and 33 ppm CO_2 within the fluid inclusions, which provides a molar ratio [H_2O / (H_2O + CO_2)] of ~0.76.

5. Discussion

As highlighted in the introduction, no dating of diamondite formation has yet been accomplished. The primary objective of this study is to measure the nitrogen concentration and aggregation states of fragments of diamondite samples to investigate their mantle residence age - average temperature relationship. To do that, we first must assume that the diamond samples analysed have grown via octahedral growth (spiral / dislocation growth; Sunagawa 2005). The

age/temperature relationship utilized below is based upon factors (i.e. activation energies, platelet formation rates) that have only been quantified specifically for octahedral diamond growth. Importantly, the available data for these samples show open cavities to contain octahedral or stepped-octahedral diamond crystal faces (Kurat and Dobosi 2000; Dobosi and Kurat 2010).

Another key assessment that must be made before interpreting the nitrogen data is whether the nitrogen aggregation data have been affected by crystal plastic deformation, which Rubanova et al. (2012) have shown is present within samples from the same collection. The exact affects of plastic deformation on the nitrogen aggregation process are unknown. Some have postulated that it enhances the rate at which aggregation occurs (Evans 1992), while others suggest it would break up the B centers into other defects (Byrne et al. 2012) thereby reducing the quantified aggregation state. Either way, to have confidence in our interpretations of the nitrogen aggregation data in terms of their age – temperature relationship, we must rule out interference of this process by plastic deformation. To do this, we use the platelet data.

With the exception of Dia068 and Dia070 (both predominantly IaA), all of the samples exhibit significant platelet development (Figure 3). Due to the high nitrogen concentrations and aggregation states, very large platelet features are often present. Figure 4 shows a "regularity" plot (after Woods 1986) of absorption due to B centers (μB) against intensity (integrated area) of the platelet band [I(B´)]. The general trend of the data is in keeping with *regular* samples as defined by Woods (1986).

197 This implies that the platelets, formed during the A to B center aggregation process,
198 have suffered no subsequent degradation (by either heating and/or deformation
199 processes). This means that we can interpret the nitrogen aggregation data with
200 confidence that the nitrogen aggregation states have not been altered by
201 deformation during residence in the mantle. While this might initially appear
202 contradictory to the work of Rubanova et al. (2012), who reported samples from
203 this same collection exhibited significant crystal plastic deformation, they also
204 showed that highly deformed diamond grains could be in contact with others
205 exhibiting little or no sign of deformation. While this would appear to confirm that
206 differential stresses are not homogeneously distributed throughout polycrystalline
207 materials (Callister 1985; Kalidindi et al. 2003), it cannot be ruled out that there was
208 an additional growth event that occurred after deformation. It is also important to
209 note that crystals containing inclusions and other defects are more susceptible to
210 the effects of deformation. The grains analysed in this study were chosen for their
211 optical transparency and therefore less likely to contain inclusions. In summary, we
212 do not rule out that the diamondites that our fragments have been taken from could
213 have been subject to plastic deformation. However, the *regular* characteristics of the
214 platelet data (after Woods, 1986) suggest that nitrogen impurity characteristics of
215 these grains have not been obviously affected by plastic deformation, and therefore
216 allow for some qualitative interpretation to be performed on them with reasonable
217 confidence.

218 More detailed interrogation of the platelet data provides an interesting result.
219 Sumida and Lang (1988) showed that larger I(B´) values are indicative of the

platelets having a greater total area per unit volume, while Clackson et al. (1990) showed that the B´ band occurring at lower wavenumbers was indicative of the platelets having a larger mean radius. The platelet data in this study (Figure 5) show that the intensity and position of the band's maximum exhibit a positive correlation, i.e. the larger intensities occur at high wavenumbers. This means that the larger population densities contain platelets of smaller sizes. This result appears to contrast with samples studied by Woods (1986) that showed no dependence of the I(B´) values on the peak position.

5.1 Nitrogen Aggregation Characteristics

The nitrogen concentrations of the studied diamondites range from 386 to 2677 ppm, while their levels of nitrogen aggregation show the full range from 100% IaA to 100% IaB. These nitrogen concentrations are relatively high compared to the average values for P and E-type monocrystalline diamonds (200 and 300 ppm respectively; Cartigny 2005), but are comparable to fibrous diamonds and diamondites globally (average = 600-800 ppm; Mikhail et al. 2013 and references therein). The largest variation in nitrogen concentration between fragments from the same diamondite sample is 916 ppm for sample Dia073B and Dia073W (where B and W refers to the black and white appearance of these fragments). Such a large range for the nitrogen concentration within a single sample is not atypical for diamond because there is no statistically significant average, i.e. the internal range of nitrogen contents within single diamonds can be anywhere between <10 and >5000 ppm; Boyd et al. 1987; Bulanova et al. 2002; Fitzsimons et al.,1999; Harte et

al. 1999; Hauri et al., 2002; Howell et al. 2012b; 2013; Mikhail et al. accepted; Smart et al. 2012; Wiggers de Vries et al. 2012). Interestingly, the nitrogen aggregation states for these samples are fairly consistent despite the large range of nitrogen concentrations within some samples (Table 1). It is clear when these nitrogen data are plotted against each other (Figure 2), the samples fall in to two discernable groups; one with low aggregation levels (Dia068 and Dia070) and the other with more developed aggregation states (40 – 100% IaB). While two samples (Dia057 and Dia075) exhibit 100% IaB aggregation and could be classified as a third group, the analytical uncertainties on the data mean they overlap with the upper end of the second group.

A diamond's nitrogen concentration and aggregation state are related to each other by the duration and average temperature at which they have resided in the mantle (Chrenko et al. 1977; Evans and Harris 1989; Mendelssohn and Milledge 1995). Isotherms are lines that correlate these two nitrogen characteristics for a fixed age and temperature. The dark grey area shown in Figure 2, which includes the data from the six samples with varied aggregation levels (42 – 94% IaB), is bound by two isotherms; the possible variations of age and temperature used to calculate these upper and lower bounds are shown in Table 2. It is clear from the values calculated in Table 2 that nitrogen aggregation is far more sensitive to temperature than age (220 - 245^{o}C variation over 3 Ga). If we assume a relatively hot geotherm (42 mW/m^2 surface heat flow; Stachel and Harris 2008), these temperatures equate to approximately 170 – 180 km at 3 Ga, and 240 – 270 km at 1 Ma. A cooler geotherm would require much greater depths to achieve these temperatures.

It is not really possible to constrain the time – temperature conditions of the two diamonds with 100% IaB aggregation states. As there is no aggregation beyond the B center stage, it cannot be determined how long they have been fully aggregated for; the calculation assumes that diamond is removed from the mantle as soon as it reaches a 100% IaB aggregation state, therefore both age and temperature determinations (when the other factor is fixed) represent minimum values. A relative comparison between these two samples and the six intermediate samples suggests that the fully aggregated samples either resided at slightly higher temperatures than the other samples (and therefore greater depths), or they have resided in the mantle for a longer period of time. Nevertheless, as these values are minimums, the differences could be much more pronounced.

As three fragments from the two samples with low aggregation levels have a value more than 0% IaB it is possible to calculate isotherms that bound the data (light grey area in Figure 2). The time and temperature values for these isotherms are shown in Table 2. Using the same geotherm as previously, these temperatures correspond to approximate depths of 135 – 160 km at 3 Ga (generally within the graphite stability field), and 180 – 215 km at 1 Ma.

In summary, the nitrogen FTIR characteristics recorded in these 10 diamondite samples cover the full range of aggregation, from pure IaA to pure IaB. These data can be interpreted in two ways. If it were assumed that all the diamondites formed at a similar time, then they would have had to grow and reside at different depths within the mantle with a relative depth range of 45 to 90 km between these samples.

Alternatively, if the diamondites all resided at similar depths in the mantle, then they would have to have formed during multiple events over a large period of time (possibly up to 3 Ga). These two outcomes imply different things about diamondite forming fluids; the exact conditions that result in diamondite formation (pressure, temperature, oxygen fugacity, carbon supersaturation, impurities) can either occur fairly simultaneously over a large vertical profile, or alternatively, occur multiple times over a large time frame. We acknowledge the two possibilities are discrete variables; more likely, a combination of both of these factors can produce diamondites at different times and depths.

5.2 Chemistry of diamondite forming fluids

While the focus of this study was on the nitrogen FTIR characteristics of the diamond material that make up diamondites, one analysis showed clear evidence of containing fluid inclusions. The molar ratio of H_2O:CO_2 of ~0.76 is in keeping with values measured in fluid inclusion rich fibrous diamonds (occurring either as fibrous cubes or fibrous coats on octahedral cores) studied by Navon et al. (1988; from Jwaneng, DRC and unknown), Schrauder and Navon (1994; Jwaneng), Tomlinson et al. (2005; DRC) and Klein-BenDavid et al. (2006; 2007; Diavik). These values, which indicate a higher water proportion, have the same basic characteristics as the silicic and saline end-member monocrystalline diamond-forming fluids (which have a H_2O:CO_2 mole ratio of 0.9 - 0.5, while the carbonatitic end-member has values <0.5; Klein-BenDavid et al. 2007)

308). Interestingly, trace element patterns in diamondites (from the same sample batch
309 as our samples) show evidence for similar parental fluid compositions to those
310 observed in fibrous diamonds (based on major and trace element abundances; see
311 Rege et al. 2008). These data suggest similar fluid-compositions are responsible for
312 the formation of both diamondite and fibrous diamonds. In support of this, highly
313 porous fibrous cubes have been observed in diamondites (Kurat and Dobosi 2000).
314 Conversely, the average carbon isotope values of diamondite and fibrous diamonds
315 are completely distinct, where these diamondites and all fibrous diamonds show a
316 mean $\delta^{13}C$ values of -18 and -5 ‰ respectively (see Mikhail et al., 2013 and
317 references therein). Therefore, a better understanding of how polycrystalline
318 diamonds fit in to diamond growth mechanism model of Sunagawa (1990, 2005)
319 would help to tie all these discrete aspects of their formation into the bigger picture
320 of not just monocrystalline diamond formation, but of C-O-H rich melts / fluids in
321 the mantle (age, temperature, oxygen fugacity, source of the diamond-forming
322 carbon etc.).

323 **6. Implications**

324 The mantle residence time for the 10 diamondites shown here can be interpreted as
325 being highly variable. An alternative interpretation is that they resided over a large
326 depth range. Considering their formation is from small-scale melt processes, this
327 would probably require multiple growth events occurring over a large depth range
328 at the same time. As the first interpretation requires multiple growth events over a
329 large time frame, it is clear that the data indicates that diamondite formation has

occurred in multiple events. This would mean the formation histories of diamondites might be more akin to the formation of monocrystalline diamonds, both in terms of time (from the nitrogen aggregation data) but also in terms source fluid chemistry (from the fluid inclusions). Constraining the relationship, or lack thereof, between monocrystalline diamonds (specifically gem quality) and diamondites could be useful to the mining industry by being able to predict the potential grade of a kimberlite. For example, is there any significance in the fact that Orapa (Botswana), one of the world's most productive diamond mines, produces a high proportion of non-profitable diamondites (Gurney and Boyd 1982)?

Constraining this relationship will most likely be best achieved by performing detailed, *in situ* geochemical analyses coupled with temporal constraints on diamondites from known geographical localities, where multiple data are available for other diamond-types.

7. Acknowledgements

This study was performed on 'left over' fragments of diamondites provided to SM by the late professor Gero Kurat for a stable isotope study performed before his passing (now published; Mikhail et al., 2013). The authors acknowledge comments from Oded Navon and Dorrit Jacob on a previous version of this manuscript, which helped to improve it. SM acknowledges funding for this study through a Carnegie postdoctoral fellowship at the Geophysical Laboratory, Washington DC, USA. This is contribution 385 from the ARC Centre of Excellence for Core to Crust Fluid Systems (http://www.ccfs.mq.edu.au) and 922 in the GEMOC Key Centre

(http://www.gemoc.mq.edu.au). FM acknowledges support from the NASA Cosmochemistry program during this work (NNX11AG76G).

8. References cited

Aulbach, S., Stachel, T., Viljoen, K.S., Brey, G.P., and Harris, J.W. (2002) Eclogitic and websteritic diamond sources beneath the Limpopo Belt-is slab-melting the link? Contributions to Mineralogy and Petrology, 143, 56.

Burgess, R., Johnson, L.H., Mattey, D.P., Harris, J.W., and Turner, G. (1998) He, Ar and C isotopes in coated and polycrystalline diamonds. Chemical Geology, 146, 205-217.

Byrne , K.S., Anstie, J.D., Chapman, J., and Luiten, A.N. (2012) Infrared microspectroscopy of natural Argyle pink diamonds. Diamond and Related Materials, 23, 125-129.

Callister, W.,(1985) Materials Science and Engineering, An Introduction. John Wiley & Sons, New York.

Cartigny, P. (2005) Stable isotopes and the origin of diamond. Elements 1, 79-84.

Chrenko, R. M., Tuft, R. E., and Strong, H. M. (1977) Transformation of the state of nitrogen in diamond. Nature 270, 141-144

Clackson SG, Moore M, Walmsley JC, and Woods GS. (1990) The relationship between platelet size and frequency of the B' infrared absorption peak in type Ia diamond. Philosophical Magazine B, 62, 115–128

Connell, S.H., Sellschop, J.P.F., Butler, J.E., Maclear, R.D., Doyle, B.P., and Machi, I.Z. (1998) A study of the mobility and trapping of minor hydrogen concentrations in diamond in three dimensions using quantitative ERDA microscopy. Diamond and Related Materials, 7, 1714-1718.

Davies, G. (1976) The A nitrogen aggregate in diamond - its symmetry and possible structure. Journal of Physics C-Solid State Physics 9, L537-L542.

Dobosi, G., Kurat, G. (2002) Trace element abundances in garnets and clinopyroxenes from diamondites - a signature of carbonatitic fluids. Mineralogy and Petrology 76, 21-38.

Dobosi, G., Kurat, G. (2010) On the origin of silicate-bearing diamondites. . Mineralogy and Petrology 99, 29–42.

Dyer HB, Raal FA, du Preez L, and Loubser JHN. (1965) Optical absorption features associated with paramagnetic nitrogen in diamond. Philosophical Magazine, 11, 763–774

Evans, T. (1992) Aggregation of nitrogen in diamond. In: Field, J.E. (Ed.), The properties of natural and synthetic diamond. Academic Press, London, pp. 259–290.

Evans, T., Harris, J.W. (1989) Nitrogen aggregation, inclusion equilibration temperatures and the age of diamonds. Special Publication Geological Society of Australian Journal of Earth Sciences 14, 1001-1006.

Evans, T., Qi, Z. (1982) The Kinetics of the Aggregation of Nitrogen-Atoms in

Diamond. Proceedings of the Royal Society of London Series a- Mathematical Physical and Engineering Sciences 381, 159.

Gautheron, C., Cartigny, P., Moreira, M., Harris, J.W., and Allegre, C.J. (2005) Evidence for a mantle component shown by rare gases, C and N isotopes in polycrystalline diamonds from Orapa (Botswana). Earth and Planetary Science Letters, 240, 559-572.

Gurney, J.J., Boyd, S.R. (1982) Mineral Intergrowths with Polycrystaline Diamonds from the Opara Mine, Botswana, Carnegie Inststitute of Washington Yearbook, Washington, pp. 267-273.

Heaney, P.J., Vicenzi, E.P., and De, S. (2005) Strange Diamonds: The Mysterious Origins of Carbonado and Framesite. Elements 1, 85-89.

Honda, M., Phillips, D., Harris, J.W., and Yatsevich, I. (2004) Unusual noble gas compositions in polycrystalline diamonds: preliminary results from the Jwaneng kimberlite, Botswana. Chemical Geology, 203, 347-358.

Howell, D., O'Neill, C.J., Grant, K.J., Griffin, W.L., Pearson, N.J., O'Reilly, S.Y., Stern, R.A., and Stachel, T. (2012a) Platelet development in cuboid diamonds: insights from micro-FTIR mapping. Contributions to Mineralogy and Petrology, 164, 1011-1025.

Howell, D., O'Neill, C.J., Grant, K.J., Griffin, W.L., Pearson, N.J., and O'Reilly, S.Y. (2012b) μ-FTIR mapping: distribution of impurities in different types of diamond growth. Diamond and Related Materials, 29, 29–36

411 Howell, D., Griffin, W., Piazolo, S., Say, J.M., Stern, R.A., Stachel, T., Nasdala, L., Rabeau,
412 J.R., Pearson, N., O'Reilly, S.Y. 2013a. A spectroscopic and carbon-isotope study of
413 mixed-habit diamonds: Impurity characteristics and growth environment. American
414 Mineralogist. 98, 66–77.

415 Humble, P., 1982. The structure and mechanism of formation of platelets in natural
416 type Ia diamond. Proceedings of the Royal Society London, A 381, 65-81.

417 Jacob, D.E., Viljoen, K.S., Grassineau, N., and Jagoutz, E. (2000) Remobilization in the
418 Cratonic Lithosphere Recorded in Polycrystalline Diamond. Science, 289, 1182-
419 1185.

420 Jacob, D.E., Kronz, A., and Viljoen, K.S. (2004) Cohenite, native iron and troilite
421 inclusions in garnets from polycrystalline diamond aggregates. Contributions to
422 Mineralogy and Petrology, 146, 566-576.

423 Jacob, D.E., Wirth, R., Enzmann, F., Kronz, A., and Schreiber, A. (2011) Nano-inclusion
424 suite and high resolution micro-computed-tomography of polycrystalline diamond
425 (framesite) from Orapa, Botswana. Earth and Planetary Science Letters, 308, 307-
426 316.

427 Kalidindi, S.R., Bhattacharyya, A., and Doherty, R.D. (2003) How do polycrystalline
428 materials deform plastically? Advanced Materials, 15 (16), 1345-1348.

429 Kirkley MB, Gurney JJ, and Rickard RS. (1991) Jwaneng framesites: carbon isotopes
430 and intergrowth compositions. In: Proceedings of the Fifth International Kimberlite

Conference, Araxá. CPRM Special Publication, 127–135.

Klein-BenDavid, O., Wirth, R., and Navon, O. (2006) TEM imaging and analysis of microinclusions in diamonds: A close look at diamond-growing fluids. American Mineralogist, 91, 353-365.

Klein-BenDavid, O., Izraeli, E.S., Hauri, E., and Navon, O. (2007) Fluid inclusions in diamonds from the Diavik mine, Canada and the evolution of diamond-forming fluids. Geochimica et Cosmochimica Acta, 71, 723-744.

Kurat, G., Dobosi, G. (2000) Garnet and diopside-bearing diamondites (framesites). Mineralogy and Petrology, 69, 143-159.

Maruoka, T., Kurat, G., Dobosi, G., and Koeberl, C. (2004) Isotopic composition of carbon in diamonds of diamondites: record of mass fractionation in the upper mantle. Geochimica Et Cosmochimica Acta, 68, 1635-1644.

Mason, H.E., McCubbin, F.M., Smirnov, A., and Phillips, B.L. (2009) Solid-state NMR and IR spectroscopic investigation of the role of structural water and F in carbonate-rich fluorapatite. American Mineralogist, 94(4), 507-516.

McCandless, T.E, Kirkley, M.B, Robinson, D.N, Gurney, J.J, Griffin, W.L, Cousens, D.R, and Boyd, F.R. (1989) Some initial observations on polycrystalline diamonds mainly from Orapa. Extended abstracts, Workshop on diamonds, 28th international geological congress, July 15-16, Washington DC, 47-51.

Mendelssohn, M.J., Milledge, H.J. (1995) Geologically significant information from

451 routine analysis of the mid-infrared spectra of diamonds. International Geology
452 Review 37, 95-110.

453 Mikhail, S., Dobosi, G., Verchovsky, A.B., Kurat, G., and Jones, A.P. (2013) Peridotitic
454 and websteritic diamondites provide new information regarding mantle melting and
455 metasomatism induced through the subduction of crustal volatiles. Geochimica Et
456 Cosmochimica Acta, 107, 1-11

457 Navon, O., Hutcheon, I.D., Rossman, G.R., and Wasserburg, G.J. (1988) Mantle-derived
458 fluids in diamond micro-inclusions. Nature, 335, 784-789.

459 Rubanova, E.V., Piazolo, S., Griffin, W.L., and O'Reilly, S.Y. (2012) Deformation
460 microstructures reveal a complex mantle history for polycrystalline diamond,
461 Geochemistry, Geophysics and Geosystems, 13, 10.

462 Schrauder, M., Navon, O. (1994) Hydrous and carbonatitic mantle fluids in fibrous
463 diamonds from Jwaneng, Botswana. Geochimica Et Cosmochimica Acta, 58, 761-771.

464 Sobolev, N.V. (1977) Deep-seated inclusions in kimberlites and the problem of the
465 composition of the upper mantle. (Translated from the Russian edition, 1974).
466 American Geophysical Union, Washington DC. 279 pp.

467 Stachel, T., Harris, J.W. (2008) The origin of cratonic diamonds – constraints from
468 mineral inclusions. Ore Geology Review, 34, 5-32.

469 Sumida, N., Lang, A.R. (1988) On the Measurement of Population-Density and Size of
470 Platelets in Type-Ia Diamond and Its Implications for Platelet Structure Models.

Proceedings of the Royal Society of London Series a- Mathematical Physical and Engineering Sciences, 419, 235.

Sunagawa, I. (1990) Growth and morphology of diamond crystals under stable and metastable conditions. Journal of Crystal Growth, 99, 1156-1161.

Sunagawa, I. (2005) Crystals: Growth, Morphology, & Perfection. Cambridge University Press, U.K.

Tomlinson, E., De Schrijver, I., De Corte, K., Jones, A.P., Moens, L., and Vanhaecke, F. (2005) Trace element compositions of submicroscopic inclusions in coated diamond: A tool for understanding diamond petrogenesis. Geochimica Et Cosmochimica Acta 69, 4719-4732.

Weiss, Y., Griffin, W.L., and Navon, O. (2013) Diamond-forming fluids in fibrous diamonds: the trace element perspective. Earth and Planetary Science Letters, 376, 110-125.

Woods, G.S. (1986) Platelets and the Infrared-Absorption of Type-Ia Diamonds. Proceedings of the Royal Society of London Series a- Mathematical Physical and Engineering Sciences, 407, 219-238.

Woods, G.S., Collins, A.T. (1983) Infrared absorption spectra of hydrogen complexes in Type I diamonds. Journal of Physics and Chemistry of Solids, 44 (5), 471-475.

Figure Captions:

Figure 1: Representative images of diamondite from this study showing some important features. (a) Sample Dia063 shows translucent and opaque regions in the same sample where the translucent regions contain a lower abundance of intergrowths and inclusions. (b) Sample Dia074 is almost totally translucent whereas (c) sample Dia073 mostly resembles a rock in appearance (i.e. totally opaque), however upon breaking the sample some fragments were more opaque than other, this lead us to use the extensions B (black) and W (white) to denote the overall transparency.

Figure 2: A plot of nitrogen concentrations vs. aggregation state for all the analyses recorded in this study. The light and dark grey areas are each defined by two isotherms that are calculated for the mantle residence ages and corresponding temperatures stated in Table 2. The isotherms are calculated using the equation $T(^{o}C) = \frac{-E}{R} \frac{1}{\ln\left[\frac{\left(\frac{C_0}{C} - 1\right)}{C_0 t A}\right]} - 273.15$ where T is the average mantle residence temperature, t is the mantle residence time in seconds, C_0 is the total nitrogen concentration of the diamond, C is the nitrogen concentration in the form of A centres, E is the activation energy and R is the gas constant (where –E/R = -81160), and A is the Arrhenius constant (2.94×10^5 s^{-1} ppm^{-1}).

Figure 3: IR spectra from samples Dia066_2, Dia068_3 and Dia073W_1, showing a range of nitrogen concentrations, aggregation states (labeled A and B), platelet intensities (labeled B′), hydrogen bands (labeled C-H) and evidence of fluid

511 inclusions (labeled OH and CO_3). Each full spectrum is presented on the same
512 absorbance scale, just offset from one another. The two insets of samples Dia066_2
513 and Dia073W_1, are presented at different scales, to highlight the fluid components
514 and nitrogen characteristics respectively.

515 Figure 4: Regularity plot (after Woods 1986) showing absorption due to B centers
516 (μ_B) *vs.* the integrated area of the platelet band (I(B´)). The black line shows the
517 regular trend as defined by Woods (1986). Some representative analytical
518 uncertainties are shown.

519 Figure 5: Graph showing the intensity *vs.* the peak position of the platelet band. The
520 data show a positive relationship indicating that the larger population densities
521 contain platelets of smaller sizes.

522 Table Captions:

523 Table 1: FTIR data for the samples in this study; nitrogen concentration (ppm),
524 aggregation state (% IaB, i.e. proportion of the total nitrogen in the diamond in the
525 form of B centers), height of the H band at 3107 cm^{-1}, integrated area of the B´
526 platelet band (cm^{-2}), and the wavenumber position of the B´ band maximum. Each
527 analysis for a given sample was performed on a different diamond fragment of the
528 given sample. The data used to assign paragenesis can be found in Dobosi and Kurat
529 (2010). The IR spectra were deconvoluted using the excel version of the DiaMap
530 software (Howell et al. 2012a, b). Uncertainties on each component are as such;
531 nitrogen content and aggregation state – ± 10%, platelet intensity [I(B´)] – ± 20%,

532 platelet band position and height – ± 1cm^{-1}, hydrogen-related band heights at 3107

533 and 1405 cm^{-1} – ± 1cm^{-1}.

534 Table 2: Calculated mantle residence temperatures for defined ages that produce the

535 isotherms that bracket the light and dark grey areas in Figure 2.

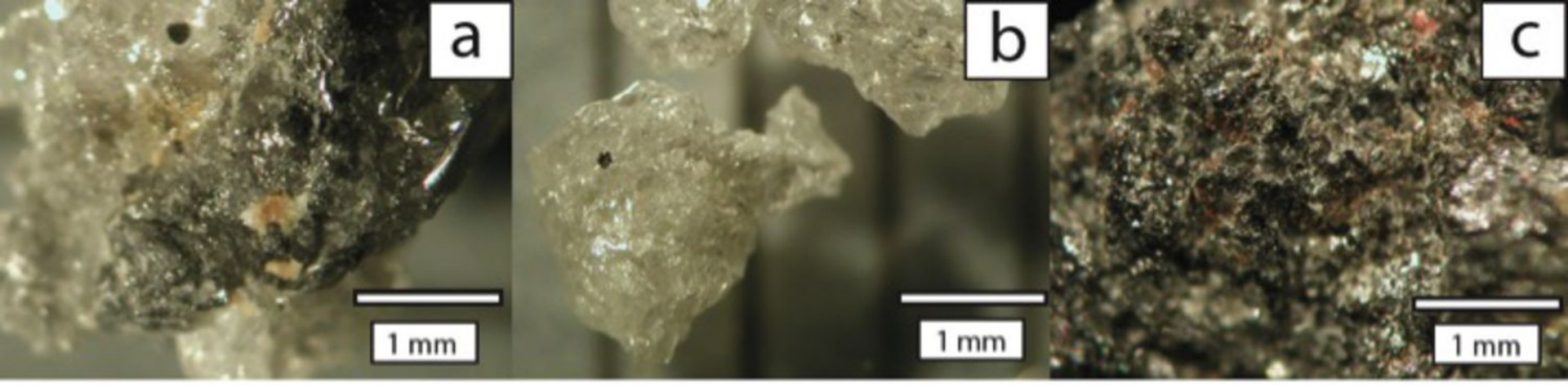
a
1 mm
b
1 mm
c
1 mm

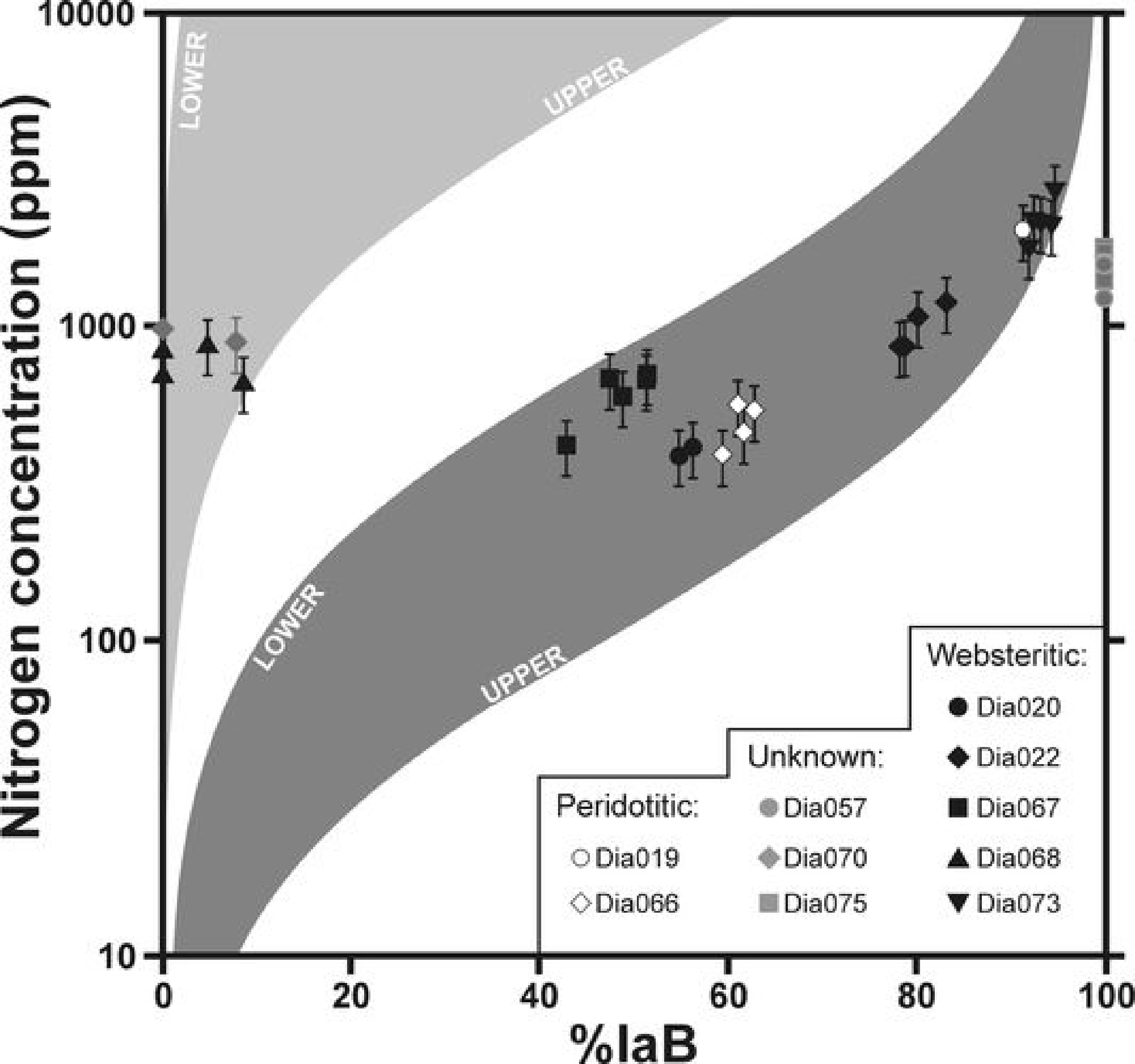
10000
1000
100
10
Nitrogen concentration (ppm)
LOWER
UPPER
LOWER
UPPER
0
20
40
60
80
100
%IaB
Websteritic:
Dia020
Unknown:
Dia022
Peridotitic:
Dia057
Dia067
Dia019
Dia070
Dia068
Dia066
Dia075
Dia073

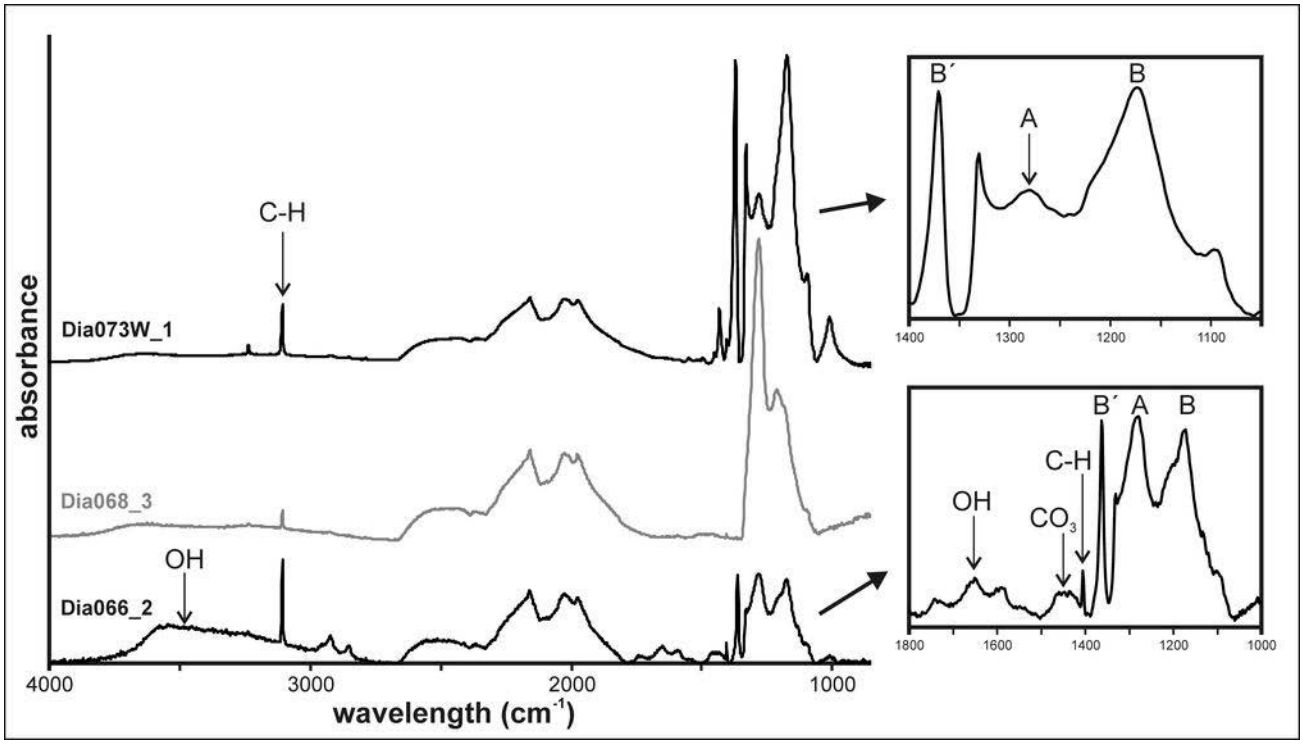
absorbance
C-H
Dia073W_1
Dia068_3
OH
Dia066_2
4000
3000
2000
1000
wavelength (cm-1)
B´
A
B
1400
1300
1200
1100
B´ A B
C-H
OH
CO3
1800
1600
1400
1200
1000

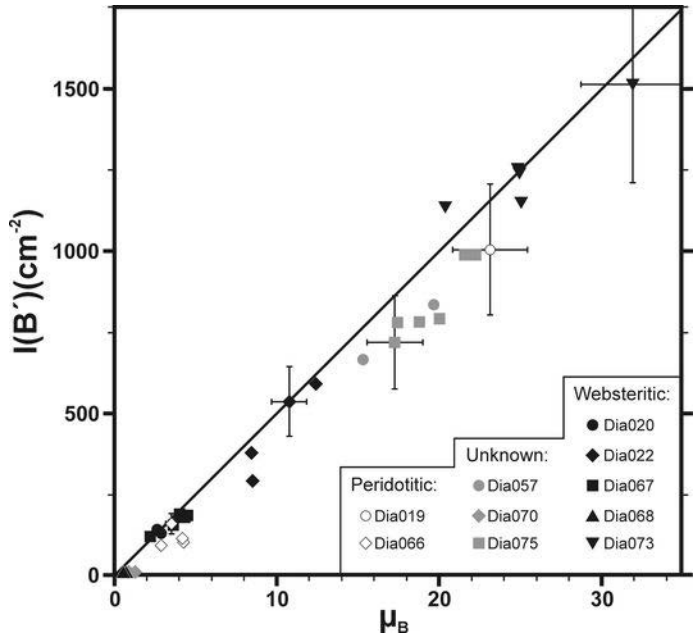
I(B´)(cm-2)
1500
1000
500
0
0
10
20
30
μB
Websteritic:
Dia020
Dia022
Unknown:
Dia057
Dia067
Peridotitic:
Dia019
Dia070
Dia068
Dia066
Dia075
Dia073

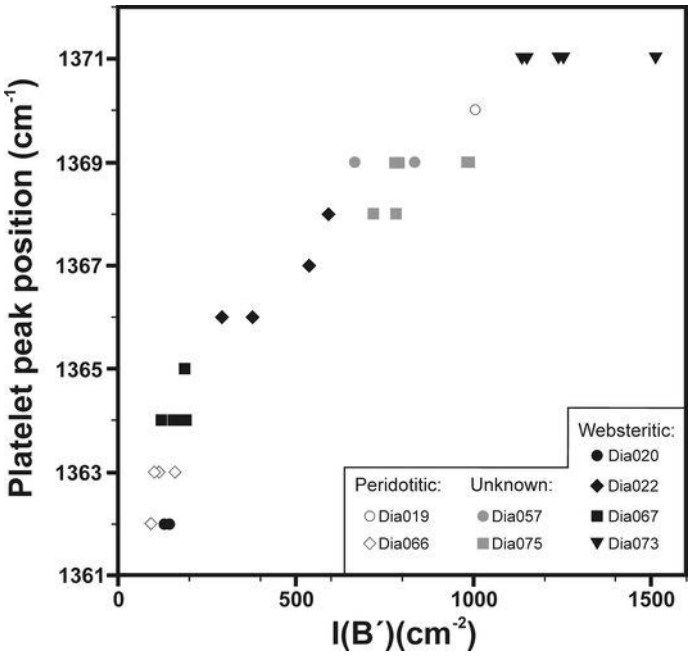
Platelet peak position (cm-1)
1371
1369
1367
1365
1363
1361
0
500
1000
1500
I(B´)(cm-2)
Websteritic:
Dia020
Dia022
Dia067
Dia073
Peridotitic:
Dia019
Dia066
Unknown:
Dia057
Dia075

Sample	Paragenesis	N total (ppm)	% IaB	H@3107 (cm^{-1})	I(B') (cm^{-2})	PLATELET position (cm^{-1})
Dia019_7	Peridotitic	2011	91.4	3.8	1006	1370
Dia020_6	Websteritic	386	54.8	0.0	143	1362
Dia020_8		411	56.3	2.0	133	1362
Dia022_1	Websteritic	861	78.8	8.2	293	1366
Dia022_3		1069	80.2	5.1	538	1367
Dia022_4		857	78.3	7.2	379	1366
Dia022_5		1186	83.2	4.3	592	1368
Dia057_3	Unknown	1216	100.0	3.4	666	1369
Dia057_4		1562	100.0	3.7	836	1369
Dia066_1	Peridotitic	388	59.5	6.8	94	1362
Dia066_2		454	61.7	12.5	161	1363
Dia066_5		556	61.2	1.2	104	1363
Dia066_7		533	62.9	1.4	117	1363
Dia067_1	Websteritic	678	47.4	7.9	191	1364
Dia067_2		701	51.4	2.2	188	1365
Dia067_4		672	51.3	6.7	181	1364
Dia067_6		416	42.9	1.2	126	1364
Dia067_7		595	48.8	9.5	156	1364
Dia068_2	Websteritic	663	8.6	2.5	Absent	Absent
Dia068_3		829	0.0	2.8	Absent	Absent
Dia068_5		867	4.8	3.6	Absent	Absent
Dia068_6		701	0.0	2.6	Absent	Absent
Dia70_4	Unknown	977	0.0	4.3	Absent	Absent
Dia70_5		887	7.8	2.9	Absent	Absent
Dia073B_1	Websteritic	2125	93.3	25.2	1240	1371
Dia073B_2		2677	94.7	37.3	1514	1371
Dia073W_1		2151	92.5	9.6	1150	1371

Dia073W_2		1761	91.9	10.7	1136	1371
Dia073W_3		2089	94.4	37.7	1254	1371
Dia075_1	Unknown	1591	100.0	3.5	793	1369
Dia075_2		1372	100.0	2.7	720	1368
Dia075_3		1493	100.0	2.3	783	1368
Dia075_4		1385	100.0	3.3	781	1369
Dia075_5		1767	100.0	2.5	988	1369
Dia075_6		1714	100.0	1.8	990	1369

Residence time	Average Temperature (°C)		Depth		Pressure (Gpa)	
	Lower	Upper	Lower	Upper	Lower	Upper
Dark grey						
1 Ma	1335	1410				
10 Ma	1265	1330				
100 Ma	1200	1260	174	195	4.9	5.8
500 Ma	1160	1210	150	171	4.5	5.0
1 Ga	1145	1195	145	164	4.3	4.8
2 Ga	1125	1175	138	156	4.1	4.6
3 Ga	1115	1165	135	152	4.0	4.55
Light grey						
1 Ma	1150	1275				
10 Ma	1100	1210				
100 Ma	1000	1150				
500 Ma	980	1110				
1 Ga	970	1095				
2 Ga	960	1080				
3 Ga	950	1070				